Environmental Science Nano

Magnetic In-Pd Catalysts for Nitrate Degradation

Journal:	*Environmental Science: Nano*
Manuscript ID	EN-ART-01-2020-000069.R2
Article Type:	Paper

Nitrate/nitrite water contaminants pose adverse health effects. Catalytic reduction is a promising treatment approach, if the catalytic materials can be designed to be stable and reusable. In this study, Pd nanoparticles were chemically attached to magnetic silica-coated iron oxide powder. Indium was added to the Pd surface to create the In-on-Pd sites needed for nitrate decomposition. This catalyst material was studied for the first time for nitrate catalytic reduction, and for magnetic separation and reuse. The catalyst was effective for nitrate treatment for many cycles, and the silica shell was effective at protecting iron oxide against iron leaching. This magnetic catalyst design can be appropriate for the degradation of other oxyanions.

Magnetic In-Pd Catalysts for Nitrate Degradation

*Sujin Guo[1,2], Camilah D. Powell[2,3], Dino Villagran[2,4] and Michael S. Wong[1,2,3,5,6]**

[1]Department of Civil & Environmental Engineering, Rice University, 6100 Main Street, Houston, TX 77005, [2]Nanosystems Engineering Research Center for Nanotechnology-Enabled Water Treatment, [3]Department of Chemical and Biomolecular Engineering, Rice University, 6100 Main Street, Houston, TX 77005, [4]Department of Chemistry and Biochemistry, University of Texas at El Paso, El Paso, TX 79968, [5]Department of Chemistry, Rice University, 6100 Main Street, Houston, TX 77005, [6]Department of Materials Science and NanoEngineering, Rice University, 6100 Main Street, Houston, TX 77005

***To Whom Correspondence Should Be Addressed** E-mail: mswong@rice.edu

Abstract

Magnetic catalysts offer the possibility of rapidly eliminating nitrate oxyanions, a ubiquitous drinking water contaminant, without generating a secondary waste stream. Herein, we report the synthesis of a magnetically recoverable bimetallic Pd-In material that exhibits excellent chemical stability, reusability, and high nitrate removal efficiency. This four-component catalyst (Pd-In/nFe_3O_4@SiO_2) contains nanocrystalline magnetite with a silica shell upon which indium-decorated palladium nanoparticles attach. The SiO_2 shell slowed down iron leaching from Fe_3O_4 and the bimetallic nano-domains showed nitrate reduction activity in deionized water without obvious deactivation through multiple recovery and reuse cycles. This magnetically responsive, reusable catalyst, which retained activity in simulated drinking water, can serve as a design basis for materials to degrade other oxyanion water contaminants.

Keywords: nitrate reduction; Fe_3O_4; bimetallic catalyst; magnetic

Introduction

Nitrate is a colorless, tasteless, and odorless compound known to be one of the common contaminants in natural waters.[1,2] With the recent rapid increase of agricultural and industrial activities globally, nitrate concentrations in groundwaters are surging all over the world.[3,4] Alarmingly, high levels of nitrate in drinking water could cause various health problems like methemoglobinemia and thyroid damage[5,6] and can lead to the formation of cancer-causing N-nitroso compounds in the human body.[7] Fortunately, various approaches have been investigated for the removal of nitrate from contaminated drinking water sources.[2,8–10] The two most common nitrate removal technologies for groundwaters in the U.S. are ion exchange (IX) and reverse osmosis (RO). However, both technologies merely separate nitrate from the water and does not eliminate or destroy it, leaving behind a concentrated waste stream that requires further treatment.[11]

Catalytic reduction is a promising chemical denitrification method due to its high activity and simple operation.[12,13] Nitrate can be directly converted into harmless dinitrogen over a catalytic surface by using hydrogen or other reducing agents under mild reaction conditions. Since this chemistry was first reported by Vorlop and Tacke in 1989,[13] extensive research efforts have been made for the development of novel catalysts with high activity and dinitrogen selectivity.[14–18] For example, monometallic Pd[19–22] and bimetallic and PdAu[23] catalysts have proven to be very active and selective to the reduction of nitrite to dinitrogen. Although Pd itself has very low reduction activity for nitrate,[24] its combination with certain secondary promotor metals greatly increases catalytic activity.[9,25–28] The Pd-In bimetallic combination is preferred over other compositions due to its high activity and high selectivity to dinitrogen over undesired ammonia.[29,30] Additionally, it is also more stable to hypochlorite exposure during clean-in-place treatment.[31]

Our previous studies[15,23,32] have focused on the synthesis of structure-controlled bifunctional catalysts and the mechanistic understanding of how the addition of promotor metals help improve the catalytic reduction of nitrate (and nitrite) oxyanions. Recently we reported the synthesis of colloidal In-decorated Pd nanoparticle ("In-on-Pd NPs") as a model catalyst for nitrate reduction.[15] Among other findings, reduction activity varied with volcano-shape dependence on In surface coverage, with In ensembles (with 4 to 6 atoms) as the active site for the nitrate-to-nitrite rate-limiting reaction step. The suspension form of these In-on-Pd NPs were amenable to batch kinetic experiments, but it is impractical for continuous-flow nitrate treatment.

Superparamagnetic Fe_3O_4 in the form of nanostructured powders ("nFe_3O_4") has been explored extensively as a magnetic catalyst support.[33–35] Once nFe_3O_4 is dispersed in a liquid, its high magnetic saturation and reversibly magnetic behavior lead to easy separation and manipulation under an external magnetic field.[36–39] nFe_3O_4 can be a catalyst support for the Pd-In NPs, such that the overall composite material is recovered and reused magnetically without the need for filtration or centrifugation. However, Fe_3O_4 is liable to leach iron species during use.[40,41] Fe_3O_4 itself shows some activity for the reduction of nitrate (and other oxyanions),[42–44] but the leached iron species may also be participating in the reaction.[45]

In this work, we demonstrate the concept of a magnetically recoverable nitrate reduction catalyst based on a multi-compositional design that comprises superparamagnetic nFe_3O_4, a SiO_2 shell coating, and Pd-In NPs. We show that the SiO_2 shell prevented iron leaching from occurring. We assess the nitrate reduction activity, selectivity and recoverability of the material in two water types (deionized water and simulated drinking water) and discuss the range of applicability of these magnetic denitrification catalysts.

Experimental section

Materials

All chemicals were of analytical grade and used as received without further purification. Ammonium hydroxide aqueous solution (NH_3, 28%), hydrochloric acid (HCl, 37%), 2-propanol, tetraethyl orthosilicate (TEOS), (3-aminopropyl) trimethoxysilane (APTES), sodium tetrachloropalladate(II) (Na_2PdCl_4), citric acid, ethanol (EtOH), polyvinylpyrrolidone (PVP, M_w~55,000), indium chloride tetrahydrate ($InCl_3 \cdot 4H_2O$, 97%), sodium nitrate ($NaNO_3$, >99.0%), sodium nitrite ($NaNO_2$, >97.0%), 1 wt% Pd on alumina catalyst (Pd/Al_2O_3), magnetite iron oxide nanopowder (nFe_3O_4), and modified Griess's reagent were purchased from Sigma-Aldrich. H_2 and CO_2 gases (99.99% purity) were obtained from Matheson. Nitrate (2.170 M, 10000 ppm) stock solution was prepared by dissolving proper amounts of $NaNO_3$ into deionized (DI) water and stored in the dark in a refrigerator at 4 °C. All the experiments were conducted using deionized (DI) water (>18 MΩ·cm, Barnstead NANOpure Diamond).

Synthesis and surface modification of nFe_3O_4@SiO_2

A modified Stober process was used to coat nFe_3O_4 material with a SiO_2 shell.[46] Briefly, 1 g of nFe_3O_4 was placed in 0.1 M HCl aqueous solution (50 mL) and ultrasonicated for 10 min; separated with magnet and washed with DI water; and then dispersed in a solution of ethanol (80 mL), DI water (20 mL) and concentrated ammonia aqueous solution (1.0 mL, 28 wt%). TEOS (0.9 g, 4.32 mmol) was added immediately afterwards. The mixture was stirred at room temperature for 12 h, and the resulting nFe_3O_4@SiO_2 solid was subsequently separated with a neodymium permanent magnet and washed with ethanol and water three times before its redispersion in an ethanol solution.

Next, to support immobilization of metal NPs, the $nFe_3O_4@SiO_2$ surfaces were functionalized with amine groups using 3-aminopropyl triethoxysilane (APTES), because of the strong chemical interaction between the NPs and the $-NH_2$ group. Approximately 1 g of $nFe_3O_4@SiO_2$ obtained from previous step was added to 60 mL of isopropanol in a 250-mL two-neck bottom-round glass flask via sonication in a water bath. Then a solution containing 1.5 mL APTES and 10 mL of isopropanol was added dropwise under stirring. The suspension was bubbled with N_2 gas for 30 min, and then sealed and left to stir at room temperature for 12 h. After magnetically recovering and washing with ethanol three times, the resulting amine-functionalized $nFe_3O_4@SiO_2$ was dried in a vacuum oven at 40 °C.[47]

Metal deposition on amine-functionalized $nFe_3O_4@SiO_2$

Pd NPs were synthesized using a one-step method.[48] Briefly, an aqueous solution of Pd salt was prepared by dissolving 57 mg of Na_2PdCl_4 in 3 mL of water. The solution was then mixed rapidly with 8 mL of aqueous solution containing 105 mg of PVP and 60 mg of L-ascorbic acid in a 25-mL round-bottom glass flask under continuous stirring. The flask was immersed in an oil bath and maintained at 80 °C for 4 h under continuous stirring. The solution was then cooled to room temperature, yielding approximately100 mg of Pd NPs.

An aliquot of the as-synthesized Pd NPs suspension (5.6 mL containing ~10 mg of Pd) was added to 30 mL water in a 100-mL round bottle glass flask on a shaker table. Then ~1 g of amine-functionalized $nFe_3O_4@SiO_2$ was added to the flask via sonication in a water bath. The mixture was then mechanically shaken continuously for several hours until the supernatant became clear and colorless, which meant the suspended Pd NPs were successfully immobilized on the $nFe_3O_4@SiO_2$ surface. The target loading of Pd NPs was 1 wt%.

Next, indium (In) metal was deposited by adding 215 μL of $InCl_3 \cdot 4H_2O$ (0.04 M) to the above solution and bubbling H_2 at 1 atm pressure for 30 min to reduce the In on top of Pd. The total In loading was 0.1 wt%. The Pd-In/nFe_3O_4@SiO_2 catalysts were collected with a neodymium permanent magnet and dried overnight in a vacuum oven at 40 °C. An alternative method involves the synthesis and immobilization of In-on-Pd NPs onto the nFe_3O_4@SiO_2 surface. We were unsuccessful in reliably producing a highly active catalyst in this manner, which we attributed to In oxidation during the handling of the In-on-Pd NPs.[15]

Synthesis of comparison materials

To test the importance of the SiO_2 shell, we synthesized "Pd-In/nFe_3O_4" by skipping the TEOS step, directly functionalizing nFe_3O_4 with APTES, and then carrying out the Pd NP immobilization and In deposition steps. For a non-magnetic version, we synthesized "Pd-In/Al_2O_3" through the incipient wetness method; 215 μL of 0.04 M $InCl_3 \cdot 4H_2O$ solution was mixed with 1 mL of DI water prior to contacting with 1 g of Pd/Al_2O_3 powder (1 wt% Pd). The resulting material (1 wt% Pd, 0.1 wt% In) was then air dried at 120 °C for 14 h and heated at 120 °C for 1 h under flowing H_2 gas (200 mL/min). TEM and XRD analysis showed Pd-In/Al_2O_3 to have 2.2-nm Pd particles and the gamma-alumina phase (Fig. S1 and Fig. S2). The Pd/Fe_3O_4 was prepared by immobilizing Pd NPs on Fe_3O_4 and In/Fe_3O_4 was made by adding In precursor to Fe_3O_4 with follow up reduction procedure in furnace (500 ℃, 3 hours). Table 1 lists the five catalyst compositions tested. The Pd and In content of Pd-In/nFe_3O_4@SiO_2 was confirmed to be within 2% of target loading using an inductively coupled plasma optical emission spectrometer (Perkin Elmer Optima 8300 ICP-OES) (Table 1). We assumed the Pd and/or In content of the comparison materials were also within 2% of target loading.

Table 1. Measured metal content and surface areas of nitrate reduction catalysts

Sample	**Pd wt%** [a]	**In wt%** [a]	**BET SA (m^2/g)**	**Support** material
Pd-In/ nFe_3O_4@SiO_2	1 (0.98[b])	0.1 (0.11[b])	15.5	SiO_2 on nFe_3O_4
Pd-In/nFe_3O_4	1	0.1	43.5	nFe_3O_4
Pd-In/Al_2O_3	1	0.1	-	Al_2O_3
Pd/nFe_3O_4	1	-	44.2	nFe_3O_4
In/nFe_3O_4	-	0.1	42.9	nFe_3O_4

a: Pd and In loadings estimated from precursor amounts
b: Pd and In loadings measured through ICP-OES

Preparation of simulated drinking water (SDW)

SDW contains dissolved species at concentrations typical of drinking water. The SDW composition follows the formulation based on the NSF/ANSI53 standard for challenge water (Table S1).[49]

Catalyst structure characterization

Magnetic measurements were collected using a Superconducting Quantum Interference Device (SQUID) completed with a MPMS XL (Quantum Design Inc.). Dried powder samples were weighed, wrapped in Teflon, and measured within the SQUID from -10 kOe to 10 kOe at 300 K. The resulting hysteresis curves were analyzed to determine the coercivity (H_c), magnetic remanence (M_r), and magnetic saturation (M_s) of each sample. Transmission electron microscopy (TEM) images were obtained using a JEOL 2010 transmission electron microscope operating at an accelerating voltage of 200 kV. The particle size distribution was calculated by counting at least 200 particles with ImageJ software. Crystal structure and powder phase analysis were obtained with a Rigaku diffractometer with Cu Kα radiation (Rigaku D/Max (WEST) Ultima Powder XRD)

instrument and Rigaku PDXL2 integrated powder XRD analysis software. The data was collected from 20° to 90°. The mean size of the ordered (crystalline) Fe_3O_4 domains was obtained from the Scherrer equation,[50] which can be written as:

$$L = \frac{K\lambda}{\beta cos\theta} \quad (1)$$

where L is the mean crystallize size. K is the dimensionless shape factor (0.94). λ is the x-ray wavelength (1.5418 Å), β expressing diffraction peak profile spread (the integral width of the most intensive peaks and is ~0.01 radian), and θ is the Bragg angle (2θ = 35.6 º) which represents the most intense peak of the (311) phase of magnetite.

Catalyst activity characterization

Similar to our previous experiments,[15,51] batch nitrate reduction experiments were conducted in a screw-cap bottle (125 mL, Alltech) with PTFE-sealed threads and a PTFE-silicone septum. The solid magnetic catalyst was added directly to the reactor before the H_2/CO_2 bubbling and the water (DI water or SDW) volume was 49.75 mL so that the final liquid reaction volume was 50 mL. The amount of catalyst was 50 mg in each reactor, the final catalyst charge concentration was 1000 mg/L, 10 mg Pd/L and 1 mg In/L, respectively. The solution was then bubbled simultaneously with H_2 gas (50 mL/min, to serve as reductant) and CO_2 gas (50 mL/min, to buffer the solution to a pH value of 4-6) for 15 min to displace dissolved oxygen and to fill the headspace with a hydrogen/CO_2 atmosphere (1 atm). All the catalytic reactions were conducted at room temperature (~23 °C). A schematic of the experimental setup was shown in ESI (Fig. S3).

After hydrogen and carbon dioxide bubbling, 0.25 mL of $NaNO_3$ solution (10 mg/mL) was injected into the sealed bottle to start the reaction (initial NO_3^- concentration was 50 mg-NO_3^-/L = 11.3 mg-N/L). The reaction was monitored periodically by withdrawing 1.5 mL aliquots from the reactor after using a neodymium permanent magnet to momentarily entrap the powder to one side

of the reactor. The activity of the non-magnetic Al_2O_3 supported catalysts was tested similarly as a control, except that the solid catalyst was removed through syringe filters (0.45-μm PFTE filter media) when sampling periodically. The sealed reactor was constantly agitated on a shaker table. To investigate the shaking speed on mass transfer limitation, experiments was designed with the Pd-In/Fe_3O_4 catalyst in which the shaking speed was modulated, and the results are shown in Fig. S4 in the ESI. The experiment verified that that shaking speed was found to show little effect on the reduction rate of nitrate when it was above 300 rpm, which suggested that the external diffusion limitation was not significant under current experimental set up (300 rpm shaking speed). In calculating the Weisz-Prater parameter (C_{wp}) to assess the presence of internal mass transfer effects, we found $C_{wp} \sim 3.6 \times 10^{-6}$, which was much less than 1, indicating internal mass transfer limitations were negligible for our nitrate reduction reaction system (specific details are in ESI).

The reusability and stability of the materials was evaluated by successive cycles of nitrate reduction reaction testing. After a reaction, the catalyst material was collected to the side of the reactor wall with a permanent magnet, then rinsed with DI water (50 mL). The reactor was then replenished with DI water (or SDW) and bubbling with H_2/CO_2 for 15 mins before adding nitrate (50 ppm) to start the next reaction cycle.

Nitrate concentrations were analyzed using a nitrate ion selective electrode (Cole-Parmer, lower detection limit 0.1 mg-NO_3^-/L). Nitrite concentrations were analyzed using the Griess test.[52] The ammonium concentrations were analyzed using Nessler's reagent. Typically, the reagent solution (0.2 mL), the sample solution (0.2 mL), and water (1.6 mL) were mixed together and allowed to react at room temperature for 10 min, after which no further color change was observed.[15]

The observed reaction rate constant k_{obs} (min^{-1}) was calculated by assuming pseudo first-order dependence on nitrate concentration (H_2 gas was in excess) and the linear portion of the data was fit with the model below:

$$-\frac{dC_{NO_3^-}}{dt} = k_{obs}C_{NO_3^-} \quad (2)$$

where $C_{NO_3^-}$ is the concentration of nitrate (with units of mg L^{-1}) and t is reaction time (with units of min).

The total metal-normalized reaction rate constant k_{cat} (with units of L g_{metal}^{-1} min^{-1}) was then calculated from $k_{cat}= k_{obs}/C_{cat}$ where C_{cat} is the total amount of In and Pd in the reaction medium volume (with units of g_{metal} L^{-1}).

The initial molar concentration of nitrate and the molar concentration of nitrate after time t are C_0 and C. Prior studies indicate that small amounts (~5%) of intermediate products NO and N_2O can be formed during nitrate reduction.[53,54] The selectivity to nitrite and to ammonium are:

$$S_{NO_2^-} = \left(\frac{C_{NO_2^-}}{C_0 - C}\right) \times 100\% \quad (3)$$

and

$$S_{NH_4^+} = \left(\frac{C_{NH_4^+}}{C_0 - C}\right) \times 100\% \quad (4)$$

Measurement of any leached Fe, Pd, and In during catalysis

The Pd and In content were determined through ICP-OES. The detection limit was 0.05 mg/L for both Pd and In. 0.5 mL of the sample was diluted with 4.4 mL H_2O and 0.1 mL aqua regia (2%) to analyze the dissolved ions. The dissolved iron measurement followed our previous study by using adapted procedures from the National Environmental Methods Index (NEMI).[55] Specifically,

the NEMI 3500 Fe-B (phenanthroline) method, which is well suited for field tests, was used.[56] For each sample, 0.5 mL was removed and combined with a solution containing HCl (20 μL; 38 wt% conc. aqueous solution), hydroxylamine (10 μL, 22.14 mM), ammonium acetate buffer (100 μL, 587 mM), and phenanthroline solution (40 μL, 0.31 mM). The resulting solution was vigorously agitated and then allowed to sit for 30 min before being analyzed with UV-vis spectroscopy at 510 nm (Shimazdu UV-2450 UV-Spectrophotometer).

Results and Discussion

Structural and magnetic properties

Representative TEM images for nFe_3O_4, nFe_3O_4@SiO_2 and Pd-In/nFe_3O_4@SiO_2 are shown in Fig. 1. The nFe_3O_4 were agglomerates of spheres with a mean diameter of 32±0.35 nm (Fig. 1a). The SiO_2 shell increased had a thickness of ~12 nm (Fig. 1b). In Fig. 1c, it can be clearly seen that Pd-In nanoparticles are deposited on the amino group functionalized SiO_2 surface. The $-NH_2$ groups chemically bind with the Pd species and subsequently are beneficial for the immobilization of Pd nanoparticles on the surface.[57] The corresponding particle size distributions of nFe_3O_4 and Pd-In NPs from Fig. 1c was shown in Fig. S5. Similar with our previous study, the size and morphology of Pd-In NPs almost remain the same after In reduction process.[48]

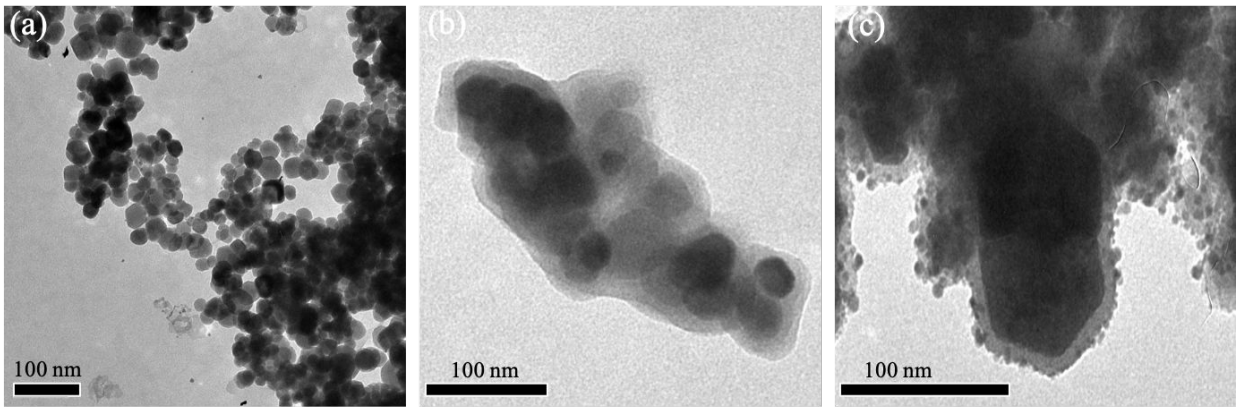

Fig. 1 (a) TEM image of nFe_3O_4, (b) $nFe_3O_4@SiO_2$ with a SiO_2 shell thickness of ~12 nm and (c) Pd-In/$nFe_3O_4@SiO_2$ catalyst.

The nFe_3O_4 powder was confirmed to be the magnetite phase (Fig. 2a). The $nFe_3O_4@SiO_2$ and Pd-In/$nFe_3O_4@SiO_2$ materials retained the magnetite phase; no additional XRD peaks were found. The grain sizes of $nFe_3O_4@SiO_2$ and Pd-In/$nFe_3O_4@SiO_2$ were ~26.8 nm and ~26.4 nm, respectively.

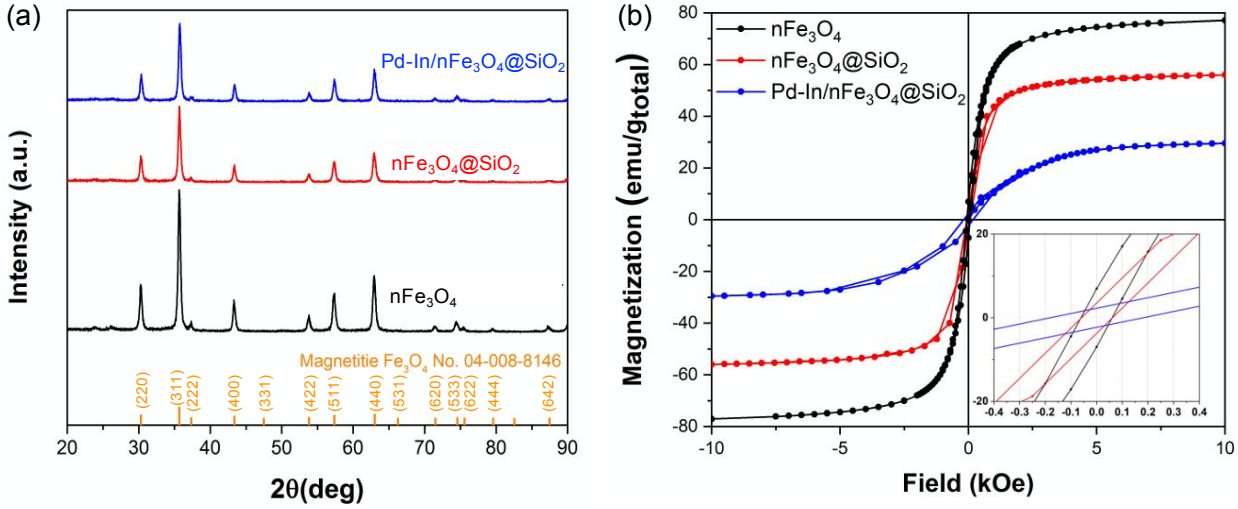

Fig. 2 (a) X-ray diffraction (XRD) pattern of nFe_3O_4, $nFe_3O_4@SiO_2$ and Pd-In/$nFe_3O_4@SiO_2$, (b) Magnetization curves of nFe_3O_4, $nFe_3O_4@SiO_2$ and Pd-In/$nFe_3O_4@SiO_2$ at 300K from -10 kOe to 10 kOe. Inset: magnetization curves from -0.4 kOe to 0.4 kOe.

The nFe_3O_4 has superparamagnetic-like behavior typical of aggregated magnetite nanoparticles, as evident by its non-zero low coercivity (*i.e.*, H_c = 0.06 kOe) and magnetic remanance (*i.e.*, 7.0 emu/g for nFe_3O_4) values (Fig. 2b). The SiO_2-coated nFe_3O_4 showed superparamagnetic-like behavior also, but its magnetic saturation M_s (56.0 emu/g_{total}) was 73% of that for nFe_3O_4 (77.1 emu/g_{total}). The magnetic saturation of the SiO_2-coated nFe_3O_4 normalized to nFe_3O_4 content (*i.e.*, 70.9 emu/g-Fe_3O_4) was below that of nFe_3O_4, pointing to contributions from the diamagnetic moments of SiO_2 atoms.[58–60] The SiO_2 shell caused SiO_2-coated nFe_3O_4 to have larger coercivity and remanance values relative to the nFe_3O_4 nanopowder.[60]

The Pd-In/nFe_3O_4@SiO_2 had a lower magnetic saturation (29.5 emu/g_{total}), 38% of that for nFe_3O_4 due to the nonmagnetic contributions of oxidized In and the SiO_2 shell. The magnetic saturation of Pd-In/nFe_3O_4@SiO_2 normalized to nFe_3O_4 content (37.4 emu/g-Fe_3O_4) was still less than that of nFe_3O_4.[61–63] Its larger coercivity value (0.18 kOe compared to 0.07 kOe for nFe_3O_4@SiO_2) may be due to Pd NPs being weakly ferromagnetic.[64] The detailed values for each sample are listed in Table S2. While its magnetic saturation was less, Pd-In/nFe_3O_4@SiO_2 can be quickly concentrated on the container wall using an external magnet, and easily redispersed into water with a manual agitation after the magnet was removed.

Nitrate reduction catalytic properties in DI water

When the reaction was completed, the catalysts were separated by using a neodymium permanent magnet. Fig. 3 shows the catalytic nitrate reduction performances by Pd/nFe_3O_4, In/nFe_3O_4, Pd-In/nFe_3O_4 and Pd-In/nFe_3O_4@SiO_2 catalysts with the same Pd (1 wt%, 10 mg/L) and In (0.1 wt%, 1 mg/L) loading amount. Pd-In/nFe_3O_4@SiO_2 and Pd-In/nFe_3O_4 showed nitrate activity comparable to that of Pd-In/Al_2O_3. Pd/nFe_3O_4 and In/nFe_3O_4 were not active, emphasizing the need for both metals.

Dinitrogen was formed as the major product (~85% at early times, ~75% towards end of reaction), with selectivities to intermediate nitrite (NO_2^-) and to ammonium (NH_4^+) of the three active catalysts are shown in Fig. S6. In general, for Pd-In/nFe_3O_4@SiO_2, and Pd-In/Al_2O_3, the selectivity to nitrite increased and then decreased as a function of nitrate conversion, with high ammonium selectivity values at higher nitrate conversions. The Pd-In/Fe_3O_4 catalyst showed slightly higher ammonium selectivity than Pd-In/Fe_3O_4@SiO_2 when the nitrate conversion above 90%, which may be due to another NO_3^-/NO_2^- reduction pathway catalyzed by leached iron (see next Section). The control sample Pd-In/Al_2O_3 generated more ammonium than the Fe_3O_4-based materials, which could be related to the average particle size of Pd being smaller on Al_2O_3 than on Fe_3O_4. Smaller particles have more low-coordination metal sites (*i.e.*, edges and corners) which impede nitrogen-containing surface species from coupling to eventually form N_2.[15,65]

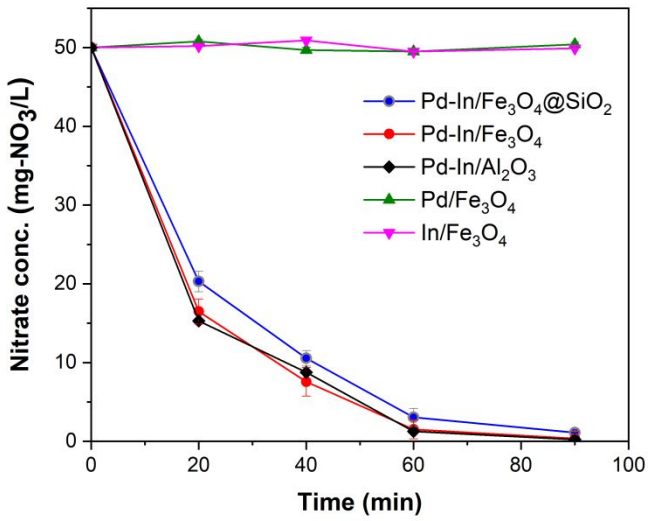

Fig. 3 Nitrate concentration-time profiles for Pd-In/nFe_3O_4@SiO_2, and for the comparison materials of Pd-In/nFe_3O_4, Pd-In/Al_2O_3, Pd/nFe_3O_4, and In/nFe_3O_4 (metal loading:1 wt% of Pd and 0.1 wt% of In). Reaction conditions: 1 g/L catalyst loading, 300 rpm string rate, 1 atm pressure, DI water containing nitrate.

Both Pd-In/nFe_3O_4 and Pd-In/nFe_3O_4@SiO_2 catalysts were magnetically recovered and reused six times. At the end of each reaction run, the catalyst in the reactor was magnetically concentrated, collected, and washed under same procedures and conditions. The decrease in nitrate concentration fit well to a pseudo first-order rate law model. The Pd-In/nFe_3O_4@SiO_2 removed >90% nitrate within 2 h for all six cycles carried out (Fig. 4a). The rate constant was 5.4 L/min/g_{metal} for the first cycle, and 4.5-4.7 L/min/g_{metal} for the last three cycles (~17% decrease). Pd-In/nFe_3O_4 showed generally similar catalytic activity (Fig. 4b). However, the rate constant increased with reaction cycle, up to ~9% in the third cycle before decreasing. Either dissolved Fe^{2+} species and the exposed Fe_3O_4 surface can increase nitrate reduction through accelerated electron transfer.[45] The uncoated Pd-In/nFe_3O_4 was apparently somewhat more active than the coated Pd-In/nFe_3O_4@SiO_2.

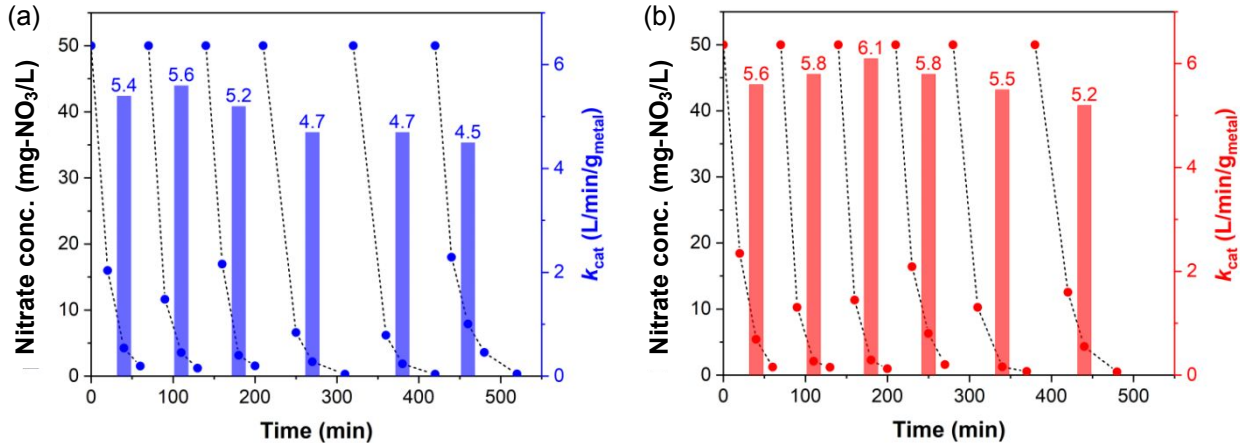

Fig. 4 Nitrate reduction kinetics in DI water for multiple recovery-reuse for (a) Pd-In/nFe_3O_4@SiO_2 and (b) Pd-In/nFe_3O_4 catalysts. Reaction conditions: 1 g/L catalyst loading, 300 rpm string rate, 1 atm pressure, DI water containing nitrate.

Chemical stability of Pd-In/nFe_3O_4@SiO_2 during nitrate reduction in DI water

Aliquots drawn from the Pd-In/nFe_3O_4@SiO_2 reaction experiments were clear and colorless when exposed to air. In contrast, yellow-colored precipitation occurred in the aliquots sampled from the

Pd-In/nFe_3O_4 reaction experiments, indicating the formation of iron oxyhydroxide and implying the leaching of dissolved iron species from the un-coated material.

The dissolved iron content was quantified during the nitrate reduction reaction through all six cycles (Fig. 5a). For the Pd-In/nFe_3O_4@SiO_2 catalyst, the dissolved iron concentration was measured to be close to or lower than the EPA secondary MCL of 0.3 mg/L. For the uncoated Pd-In/nFe_3O_4 catalyst, the dissolved iron concentration exceeded ~60 mg/L after the first cycle; this uncoated material continued to release iron through the subsequent cycles, at concentrations that were an order of magnitude higher than compared to the coated material.

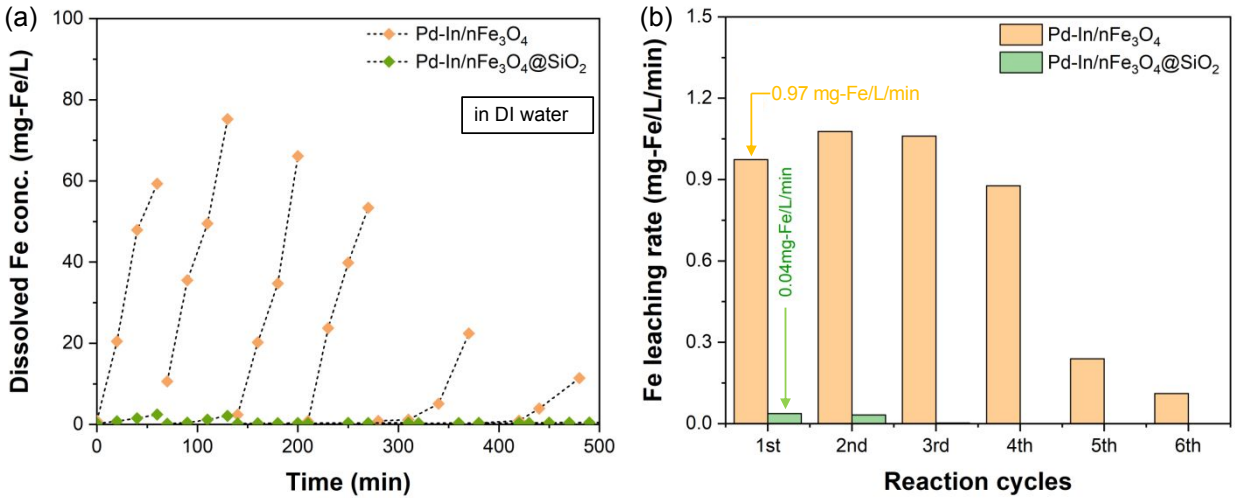

Fig. 5 (a) Total dissolved iron concentrations in DI water for multiple recovery-reuse and (b) corresponding iron leaching rate from Pd-In/nFe_3O_4 and Pd-In/nFe_3O_4@SiO_2. Reaction conditions: 1 g/L catalyst loading, 300 rpm string rate, 1 atm pressure, DI water containing nitrate.

The iron leaching rates were calculated for each cycle for both materials (Fig. 5b). In the first reaction cycle, the SiO_2 coating lowered the iron leaching rate (from 0.97 mg-Fe/L/min to 0.04 mg-Fe/L/min) by 96%, indicating the effectiveness of the SiO_2 shell to substantially suppress iron leaching from the Fe_3O_4 support. Whereas the coated material showed little leaching in subsequent

cycles (<0.002 mg-Fe/L/min), the uncoated material showed increased leaching rates in the second and third cycles, and decreased rates in subsequent reaction cycles. The presence of dissolved iron correlated with the higher rate constants of the uncoated material compared to the coated material (Fig. 4). Measurements of dissolved Pd and In for Pd-In/nFe_3O_4@SiO_2 were carried out at the end of each cycle (via ICP-OES). No leached Pd or In were detected. In summary, these results demonstrate that the Pd-In/nFe_3O_4@SiO_2 catalyst is chemically stable against iron and NP leaching and that the silica shell provides effective protection of the iron oxide support.

Testing Pd-In/nFe_3O_4@SiO_2 for nitrate reduction in simulated drinking water

The reactivity of catalysts in real water systems is strongly affected by several factors, such as (1) temporary or permanent fouling by impurities in the water, (2) loss of the promoter metal, noble metal, and/or support material due to leaching in treated discharges, and (3) damage to the material structure during regeneration treatment to recover catalyst performance.[27,30,66]

We assessed the nitrate reduction properties of Pd-In/nFe_3O_4@SiO_2 in realistic drinking water by carrying out the recovery-reuse experiments for six cycles using simulated drinking water. The catalyst was active for all cycles, but the activity was lower (Fig. 6a). The first cycle took ~200 min to reach ~90% conversion (compared to 60 min, in DI water case, Fig. 4a). The rate constants for the simulated drinking water and DI water cases were 1.3 and 5.4 L/min/g_{metal}, respectively. The catalyst became less active with recovery-reuse cycles; the rate constant was 0.7 L/min/g_{metal} at the last cycle. It expectedly showed little iron leaching after the first cycle (Fig. 4b). Less than 10 mg/L ppm iron was detected, and the leaching rate was comparably low (0.027 mg-Fe/L/min). Without the coating, the Pd-In/nFe_3O_4 experienced significant leaching after one cycle (0.45 mg-Fe/L/min, Fig. S7. Iron leaching appeared to be slower in SDW than in DI water.

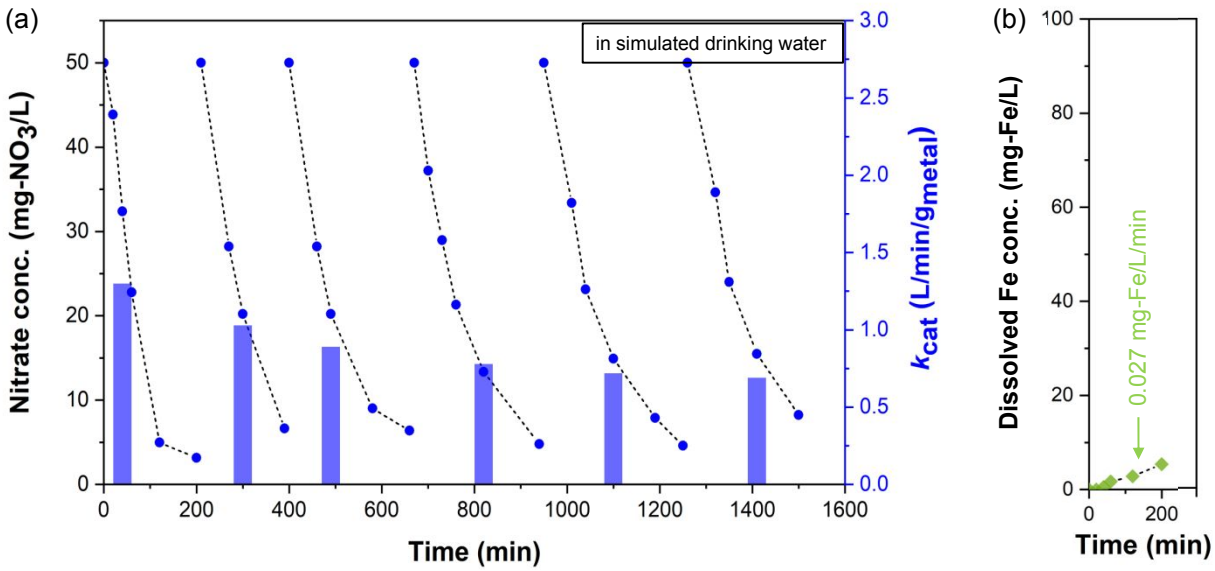

Fig. 6 (a) Nitrate reduction kinetics in SDW for multiple recovery-reuse for Pd-In/nFe_3O_4@SiO_2, and (b) the iron leaching concentration during the first cycle. Reaction conditions: 1 g/L catalyst loading, 300 rpm string rate, 1 atm pressure, SDW containing nitrate.

The catalyst likely suffered from fouling or competitive adsorption by many of the SDW constituents (Table S1). Halide ions, SO_4^{2-}, and HCO_3^- have weak interactions with the catalyst metals, and the overall reaction rate decreases when these ionic species compete with the NO_3^- species for the active site adsorption during the reduction reaction.[18,67,68] Calcium and magnesium ions are also in SDW. Mineral precipitation on the catalyst surface can result in blockage of active sites and lead to decreases in contaminant reduction rate constants. It has been reported that mineral precipitation by hardness ions (e.g., Ca^{2+} and Mg^{2+}) does not occur to a large extent during catalytic dehalogenation,[42] likely due to the generation of protons during reaction. However, mineral precipitation can foul Pd-based catalysts during catalytic NO_3^- reduction.[9,69,70] Appropriate regeneration strategies and engineering solutions (such as introducing citrate as an antiscaling agent[70]) would improve the performance stability and reusability of such catalysts.

We quantified the selectivities to nitrite and ammonium for first cycle (Fig. S8). The selectivity trends were similar to the DI water case, but the selectivity values were generally higher. At 50% nitrate conversion in SDW, S_{NO2-} and S_{NH4+} were 15% and 20%, respectively. At the same conversion, nitrate reduction in DI water yielded S_{NO2-} and S_{NH4+} values less than ~5% (Fig. S6). Carrying out the nitrate reduction reaction in SDW caused the catalyst to generate more nitrite and ammonia than in DI water. The higher nitrite and ammonium selectivities in SDW may be the result of salt species competing with nitrate anions for the same adsorption sites and displacing N-containing surface intermediate species that are needed for N-N coupling.[71,72]

Conclusions

We successfully (i) synthesized a core-shell magnetic catalyst with bimetallic Pd-In NPs attached to its surface, (ii) characterized the material through TEM and SQUID, (iii) tested its catalytic properties toward aqueous phase nitrate reduction, and (iv) performed iron leaching and magnetic recovery tests. The Fe_3O_4 allowed for the easy recovery and collection, and SiO_2 coating substantially protected the Fe_3O_4 from leaching iron during the nitrate reduction reaction. Pd and In leaching was not detected. The Pd-In/nFe_3O_4@SiO_2 nanocomposite material showed repeatable nitrate reduction performance over six recovery-reuse cycles in DI water and in SDW, with the latter lowering (but not eliminating) catalytic activity. SiO_2-coated Fe_3O_4 nanopowders are a stable, magnetically capturable material that may usefully host other catalytic NPs for water treatment reactions.

Acknowledgement

The authors gratefully acknowledge financial support from the NSF Nanosystems Engineering Research Center for Nanotechnology-Enabled Water Treatment (EEC-1449500). S.G. acknowledges financial support from the China Scholarship Council. The authors thank Dr. C. Ayala for assistance in TEM characterization, Dr. J. Li (Rice University Shared Equipment Authority) for helpful discussions about XRD analysis.

Reference

1 F. T. Wakida and D. N. Lerner, Non-agricultural sources of groundwater nitrate: A review and case study, *Water Res.*, 2005, **39**, 3–16.
2 A. Kapoor and T. Viraraghavan, Nitrate removal from drinking water-review, *J. Environ. Eng.*, 1997, **123**, 371–380.
3 A. H. Mahvi, J. Nouri, A. A. Babaei and R. Nabizadeh, Agricultural activities impact on groundwater nitrate pollution, *Int. J. Environ. Sci. Technol.*, 2005, **2**, 41–47.
4 E. V. S. Prakasa Rao and K. Puttanna, Nitrates, agriculture and environment, *Curr. Sci.*, 2000, **79**, 1163–1168.
5 L. Knobeloch, B. Salna, A. Hogan, J. Postle and H. Anderson, Blue babies and nitrate-contaminated well water, *Environ. Health Perspect.*, 2000, **108**, 675–678.
6 N. S. Bryan and H. van Grinsven, The Role of Nitrate in Human Health, *Adv. Agron.*, 2013, **119**, 153–182.
7 M. H. Ward, R. R. Jones, J. D. Brender, T. M. de Kok, P. J. Weyer, B. T. Nolan, C. M. Villanueva and S. G. van Breda, Drinking water nitrate and human health: An updated review, *Int. J. Environ. Res. Public Health*, 2018.
8 M. T. Amin, A. Alazba and U. Manzoor, A review on removal of pollutants from water / wastewater using different types of nanomaterials, *Adv. Mater. Sci. Eng.*, 2014, **2014**, 24.
9 A. E. Palomares, C. Franch and A. Corma, Nitrates removal from polluted aquifers using (Sn or Cu)/Pd catalysts in a continuous reactor, *Catal. Today*, 2010, **149**, 348–351.
10 S. Hörold, K.-D. Vorlop, T. Tacke and M. Sell, Development of catalysts for a selective nitrate and nitrite removal from drinking water, *Catal. Today*, 1993, **17**, 21–30.
11 K. N. Heck, S. Guo, P. Westerhoff and M. S. Wong, Removing Nitrates and Nitrites through New Catalysis Chemistry, *Water Cond. Purif.*, 2018, **3**, 36–40.
12 N. Barrabés and J. Sá, Catalytic nitrate removal from water, past, present and future perspectives, *Appl. Catal. B Environ.*, 2011, **104**, 1–5.
13 K. Vorlop and T. Tacke, Getting started on the road to noble metal-nitrate and nitrite from drinking water, *Chem. Eng. Technol.*, 1989, **61**, 836–837.
14 J. Martínez, A. Ortiz and I. Ortiz, State-of-the-art and perspectives of the catalytic and electrocatalytic reduction of aqueous nitrates, *Appl. Catal. B Environ.*, 2017, 207, 42–59.
15 S. Guo, K. Heck, S. Kasiraju, H. Qian, Z. Zhao, L. C. Grabow, J. T. Miller and M. S.

Wong, Insights into Nitrate Reduction over Indium-Decorated Palladium Nanoparticle Catalysts, *ACS Catal.*, 2018, **8**, 503–515.

16 X. Huo, D. J. Van Hoomissen, J. Liu, S. Vyas and T. J. Strathmann, Hydrogenation of aqueous nitrate and nitrite with ruthenium catalysts, *Appl. Catal. B Environ.*, 2017, **211**, 188–198.

17 X. Chen, X. Huo, J. Liu, Y. Wang, C. J. Werth and T. J. Strathmann, Exploring beyond palladium: Catalytic reduction of aqueous oxyanion pollutants with alternative platinum group metals and new mechanistic implications, *Chem. Eng. J.*, 2017, **313**, 745–752.

18 B. P. Chaplin, E. Roundy, K. A. Guy, J. R. Shapley and C. I. Werth, Effects of natural water ions and humic acid on catalytic nitrate reduction kinetics using an alumina supported Pd-Cu catalyst, *Environ. Sci. Technol.*, 2006, **40**, 3075–3081.

19 K. Pirkanniemi and M. Sillanpää, Heterogeneous water phase catalysis as an environmental application: a review, *Chemosphere*, 2002, **48**, 1047–1060.

20 S. D. Ebbesen, B. L. Mojet and L. Lefferts, Effect of pH on the nitrite hydrogenation mechanism over pd/Al 2O3 and Pt/Al2O3: Details obtained with ATR-IR spectroscopy, *J. Phys. Chem. C*, 2011, **115**, 1186–1194.

21 S. D. Ebbesen, B. L. Mojet and L. Lefferts, In situ ATR-IR study of nitrite hydrogenation over Pd/Al2O3, *J. Catal.*, 2008, **256**, 15–23.

22 J. K. Chinthaginjala and L. Lefferts, Support effect on selectivity of nitrite reduction in water, *Appl. Catal. B Environ.*, 2010, **101**, 144–149.

23 H. Qian, Z. Zhao, J. C. Velazquez, L. A. Pretzer, K. N. Heck and M. S. Wong, Supporting palladium metal on gold nanoparticles improves its catalysis for nitrite reduction, *Nanoscale*, 2014, **6**, 358–364.

24 F. Epron, F. Gauthard and J. Barbier, Catalytic Reduction of Nitrate in Water on a Monometallic Pd/CeO2 Catalyst, *J. Catal.*, 2002, **206**, 363–367.

25 U. Matatov-Meytal and M. Sheintuch, Activated carbon cloth-supported Pd-Cu catalyst: Application for continuous water denitrification, *Catal. Today*, 2005, **102–103**, 121–127.

26 F. Deganello, L. F. Liotta, a. Macaluso, a. M. Venezia and G. Deganello, Catalytic reduction of nitrates and nitrites in water solution on pumice-supported Pd-Cu catalysts, *Appl. Catal. B Environ.*, 2000, **24**, 265–273.

27 S. Hamid, M. A. Kumar and W. Lee, Highly reactive and selective Sn-Pd bimetallic catalyst supported by nanocrystalline ZSM-5 for aqueous nitrate reduction, *Appl. Catal. B Environ.*, 2016, **187**, 37–46.

28 K. a. Guy, H. Xu, J. C. Yang, C. J. Werth and J. R. Shapley, Catalytic nitrate and nitrite reduction with Pd-Cu/PVP colloids in water: Composition, structure, and reactivity correlations, *J. Phys. Chem. C*, 2009, **113**, 8177–8185.

29 U. Prüsse and K. D. Vorlop, Supported bimetallic palladium catalysts for water-phase nitrate reduction, *J. Mol. Catal. A Chem.*, 2001, **173**, 313–328.

30 B. P. Chaplin, M. Reinhard, W. F. Schneider, C. Schüth, J. R. Shapley, T. J. Strathmann and C. J. Werth, Critical review of Pd-based catalytic treatment of priority contaminants in water, *Environ. Sci. Technol.*, 2012, **46**, 3655–3670.

31 B. P. Chaplin, J. R. Shapley and C. J. Werth, Regeneration of sulfur-fouled bimetallic Pd-based catalysts, *Environ. Sci. Technol.*, 2007, **41**, 5491–5497.

32 Y. B. Yin, S. Guo, K. N. Heck, C. A. Clark, C. L. Coonrod and M. S. Wong, Treating Water by Degrading Oxyanions Using Metallic Nanostructures, *ACS Sustain. Chem. Eng.*, 2018, **6**, 11160–11175.

33 V. Polshettiwar, R. Luque, A. Fihri, H. Zhu, M. Bouhrara and J. M. Basset, Magnetically recoverable nanocatalysts, *Chem. Rev.*, 2011, **111**, 3036–3075.

34 H. Deng, X. Li, Q. Peng, X. Wang, J. Chen and Y. Li, Monodisperse magnetic single-crystal ferrite microspheres, *Angew. Chemie - Int. Ed.*, 2005, **44**, 2782–2785.

35 J. Liu, Z. Sun, Y. Deng, Y. Zou, C. Li, X. Guo, L. Xiong, Y. Gao, F. Li and D. Zhao, Highly water-dispersible biocompatible magnetite particles with low cytotoxicity stabilized by citrate groups, *Angew. Chemie - Int. Ed.*, 2009, **48**, 5875–5879.

36 W. Tang, Y. Su, Q. Li, S. Gao and J. K. Shang, Mg-doping: a facile approach to impart enhanced arsenic adsorption performance and easy magnetic separation capability to α-Fe $_2$ O $_3$ nanoadsorbents, *J. Mater. Chem. A*, 2013, **1**, 830–836.

37 A. H. Lu, E. L. Salabas and F. Schüth, Magnetic nanoparticles: Synthesis, protection, functionalization, and application, *Angew. Chemie-International Ed.*, 2007, **46**, 1222–1244.

38 M. B. Gawande, P. S. Branco and R. S. Varma, Nano-magnetite (Fe3O4) as a support for recyclable catalysts in the development of sustainable methodologies, *Chem. Soc. Rev.*, 2013, **42**, 3371–3393.

39 R. B. N. Baig, R. S. Varma, S. V. Ley, W. J. Stark, O. Reiser, C. F. Perno, A. Karlsson, J. Balzariniand, M. J. Camarasa, D. K. Hutchinson, J. Morris, R. J. Reischer, C. W. Ford, G. E. Zurenko, J. C. Hamel, R. D. Schaadt, D. Stapert and B. H. Yagi, Magnetically retrievable catalysts for organic synthesis, *Chem. Commun.*, 2013, **49**, 752–770.

40 L. Xu and J. Wang, Fenton-like degradation of 2,4-dichlorophenol using Fe 3O 4 magnetic nanoparticles, *Appl. Catal. B Environ.*, , DOI:10.1016/j.apcatb.2012.04.028.

41 L. Hu, P. Wang, G. Liu, Q. Zheng and G. Zhang, Catalytic degradation of p-nitrophenol by magnetically recoverable Fe3O4 as a persulfate activator under microwave irradiation, *Chemosphere*, , DOI:10.1016/j.chemosphere.2019.124977.

42 W. Sun, Q. Li, S. Gao and J. K. Shang, Highly efficient catalytic reduction of bromate in water over a quasi-monodisperse{,} superparamagnetic Pd/Fe3O4 catalyst, *J. Mater. Chem. A*, 2013, **1**, 9215–9224.

43 W. Sun, Q. Li, S. Gao and J. K. Shang, Monometallic Pd/Fe 3O 4 catalyst for denitrification of water, *Appl. Catal. B Environ.*, 2012, **125**, 1–9.

44 P. Zheng, Z. Pan and J. Zhang, Synergistic enhancement in catalytic performance of superparamagnetic Fe3O4@bacilus subtilis as recyclable fenton-like catalyst, *Catalysts*, , DOI:10.3390/catal7110349.

45 J. Xu, Z. Hao, C. Xie, X. Lv, Y. Yang and X. Xu, Promotion effect of Fe 2+ and Fe 3O 4 on nitrate reduction using zero-valent iron, *Desalination*, , DOI:10.1016/j.desal.2011.08.029.

46 W. Stöber, A. Fink and E. Bohn, Controlled growth of monodisperse silica spheres in the micron size range, *J. Colloid Interface Sci.*, 1968, **26**, 62–69.

47 Y. Deng, D. Qi, C. Deng, X. Zhang and D. Zhao, Superparamagnetic high-magnetization microspheres with an Fe 3O4@SiO2 core and perpendicularly aligned mesoporous SiO2 shell for removal of microcystins, *J. Am. Chem. Soc.*, , DOI:10.1021/ja0777584.

48 E. C. Welman, H. N. Kimberly, S. Guo, S. Yazdi, C. Ayala-Orozco, S. Grossweiler, D. B. Josiel and Emilie Ringe, Indium-decorated Pd Nanocubes Degrade Nitrate Anions Rapidly, *Appl. Catal. B Environ.*

49 NSF/ANSI 53 Standards for Water Treatment Systems, NSF/ANSI 53 Standards for Water Treatment Systems.

50 N. C. Halder and C. N. J. Wagner, Separation of particle size and lattice strain in integral breadth measurements, *Acta Crystallogr.*, , DOI:10.1107/s0365110x66000628.

51 H. Li, S. Guo, K. Shin, M. S. Wong and G. Henkelman, Design of a Pd–Au Nitrite Reduction Catalyst by Identifying and Optimizing Active Ensembles, *ACS Catal.*, , DOI:10.1021/acscatal.9b02182.

52 D. F. Boltz, *Colometric determination of nonmetals.*, *Colometric determination of nonmetals.*, John Wiley, New York, 1978.

53 R. Zhang, D. Shuai, K. a. Guy, J. R. Shapley, T. J. Strathmann and C. J. Werth, Elucidation of Nitrate Reduction Mechanisms on a Pd-In Bimetallic Catalyst using Isotope Labeled Nitrogen Species, *ChemCatChem*, 2013, **5**, 313–321.

54 B. P. Chaplin, J. R. Shapley and C. J. Werth, The selectivity and sustainability of a Pd-In/γ-Al2O3 catalyst in a packed-bed reactor: The effect of solution composition, *Catal. Letters*, 2009, **130**, 56–62.

55 C. D. Powell, S. Guo, L. M. Godret-Miertschin, K. Ventura, A. W. Lounsbury, C. A. Clark, D. Villagran, J. B. Zimmerman, A. J. Atkinson, P. Westerhoff and M. S. Wong, Magnetically recoverable carbon-coated iron carbide for arsenic adsorptive removal, *J. Nanoparticle Res.*

56 W. E. Federation, Standard Methods for the Examination of Water and Wastewater Standard Methods for the Examination of Water and Wastewater, *Public Health*, , DOI:10.2105/AJPH.51.6.940-a.

57 Y. Wang, J. Liu, P. Wang, C. J. Werth and T. J. Strathmann, Palladium Nanoparticles Encapsulated in Core − Shell Silica : A Structured Hydrogenation Catalyst with Enhanced Activity for Reduction of Oxyanion Water Pollutants, *ACS Catal.*, 2014, **4**, 3551–3559.

58 M. Veligatla, S. Katakam, S. Das, N. Dahotre, R. Gopalan, D. Prabhu, D. Arvindha Babu, H. Choi-Yim and S. Mukherjee, Effect of Iron on the Enhancement of Magnetic Properties for Cobalt-Based Soft Magnetic Metallic Glasses, *Metall. Mater. Trans. A Phys. Metall. Mater. Sci.*, , DOI:10.1007/s11661-014-2714-2.

59 S. Larumbe, C. Gómez-Polo, J. I. Pérez-Landazábal and J. M. Pastor, Effect of a SiO2 coating on the magnetic properties of Fe3O4 nanoparticles., *J. Phys. Condens. Matter*, , DOI:10.1088/0953-8984/24/26/266007.

60 Y. Cheng, R. Tan, W. Wang, Y. Guo, P. Cui and W. Song, Controllable synthesis and magnetic properties of Fe3O 4 and Fe3O4@SiO2 microspheres, *J. Mater. Sci.*, , DOI:10.1007/s10853-010-4583-4.

61 N. H. Chou, X. Ke, P. Schiffer and R. E. Schaak, Room-temperature chemical synthesis of shape-controlled indium nanoparticles, *J. Am. Chem. Soc.*, 2008, **130**, 8140–8141.

62 A. Singhal, S. N. Achary, J. Manjanna, O. D. Jayakumar, R. M. Kadam and A. K. Tyagi, Colloidal Fe-doped indium oxide nanoparticles : Facile synthesis , structural , and magnetic properties, *J. Phys. Chem. C*, 2009, **113**, 3600–3606.

63 J. Chandradass, D. S. Bae and K. H. Kim, A simple method to prepare indium oxide nanoparticles: Structural, microstructural and magnetic properties, *Adv. Powder Technol.*, 2011, **22**, 370–374.

64 M. S. Seehra, J. D. Rall, J. C. Liu and C. B. Roberts, Core-shell model for the magnetic properties of Pd nanoparticles, *Mater. Lett.*, 2012, **68**, 347–349.

65 F. Zhang, S. Miao, Y. Yang, X. Zhang, J. Chen and N. Guan, Size-dependent hydrogenation selectivity of nitrate on Fd-Cu/TiO2catalysts, *J. Phys. Chem. C*, 2008, **112**, 7665–7671.

66 J. Jung, S. Bae and W. Lee, Nitrate reduction by maghemite supported Cu-Pd bimetallic catalyst, *Appl. Catal. B Environ.*, 2012, **127**, 148–158.
67 A. Pintar, M. Šetinc and J. Levec, Hardness and salt effects on catalytic hydrogenation of aqueous nitrate solutions, *J. Catal.*, , DOI:10.1006/jcat.1997.1960.
68 L. Lemaignen, C. Tong, V. Begon, R. Burch and D. Chadwick, Catalytic denitrification of water with palladium-based catalysts supported on activated carbons, *Catal. Today*, 2002, **75**, 43–48.
69 A. J. Lecloux, Chemical, biological and physical constrains in catalytic reduction processes for purification of drinking water, *Catal. Today*, , DOI:10.1016/S0920-5861(99)00100-5.
70 J. C. Velázquez, S. Leekumjorn, G. D. Hopkins, K. N. Heck, J. S. McPherson, J. A. Wilkens, B. S. Nave, M. Reinhard and M. S. Wong, High activity and regenerability of a palladium–gold catalyst for chloroform degradation, *J. Chem. Technol. Biotechnol.*, , DOI:10.1002/jctb.4851.
71 C. A. Clark, C. P. Reddy, H. Xu, K. N. Heck, G. Luo, T. P. Senftle and M. S. Wong, Mechanistic Insights into pH-Controlled Nitrite Reduction to Ammonia and Hydrazine over Rhodium, *ACS Catal.*, 2019, **10**, 494–509.
72 H. Shin, S. Jung, S. Bae, W. Lee and H. Kim, Nitrite Reduction Mechanism on a Pd Surface, *Environ. Sci. Technol.*, 2014, **48**, 12768–12774.

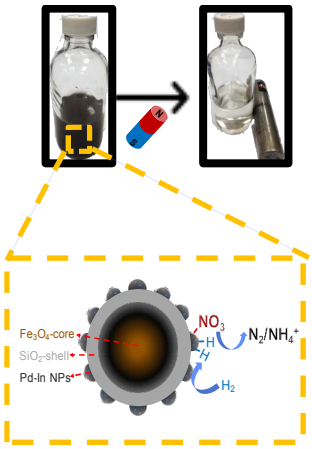
Fe3O4-core
SiO2-shell
Pd-In NPs
NO3
H
N2/NH4+
H2